

15. Recombinant retroviruses were produced by transient transfection of human embryonal kidney 293T cells:  $2 \times 10^6$  cells were plated 24 hours before transfection in 60-mm dishes. Transfection was performed by calcium-phosphate precipitation with 3  $\mu\text{g}$  of a retroviral vector (14) encoding luciferase linked to an internal ribosome entry site and a green fluorescent protein derivative (GFP; pEGFP, Clontech), pLZRs-Luc-Gfp; 5  $\mu\text{g}$  of an expression vector encoding gag and pol, pNGVL-MLVgag-pol; and 1  $\mu\text{g}$  of the envelope-encoding plasmid: pNGVL-4070A (ampho) env, pCMV-Eco env, or p1012-Ebola GP, respectively. Supernatants corresponding to 24 to 48 hours after transfection were harvested,

cleared by low-speed centrifugation, and either used immediately for infection or frozen at  $-80^\circ\text{C}$ . Infections were performed in 6-well plates ( $1.5 \times 10^5$  to  $2.5 \times 10^5$  adherent cells) or 12-well plates ( $5 \times 10^5$  nonadherent cells) with different dilutions of the supernatants by incubating the cells overnight with 1 ml and 300  $\mu\text{l}$ , respectively, of the diluted supernatants. Polybrene was used at a concentration of 5  $\mu\text{g}/\text{ml}$  for all the cell lines except for D17, for which the concentration was 100  $\mu\text{g}/\text{ml}$ . After overnight infection, fresh medium was added and the cells were incubated for an additional 24 hours. After infection, the cells were lysed in 25 mM tris-phosphate, pH 8, 2 mM dithiothreitol, 2 mM 1,2-diaminocyclohexane-

*N,N,N',N'*-tetraacetic acid, 10% glycerol, and 1% Triton X-100 and assayed for luciferase activity with Luciferase Assay Reagent (Promega, Madison, WI) in a 1251 BioOrbit Luminometer. The same number of cells (range  $5 \times 10^4$  to  $10 \times 10^4$ ) was analyzed for every specific cell line.

16. J. E. Embretson and H. M. Temin, *J. Virol.* **61**, 3454 (1987).

17. We thank S. Nichol for helpful discussions and D. Gschwend and N. Barrett for manuscript preparation. R.D. is supported by a grant of the Ministry of Education and Science of Spain.

15 October 1997; accepted 5 January 1998

## The Structure of GABP $\alpha/\beta$ : An ETS Domain–Ankyrin Repeat Heterodimer Bound to DNA

Adrian H. Batchelor, Derek E. Piper,  
Fabienne Charles de la Brousse, Steven L. McKnight,  
Cynthia Wolberger\*

GA-binding protein (GABP) is a transcriptional regulator composed of two structurally dissimilar subunits. The  $\alpha$  subunit contains a DNA-binding domain that is a member of the ETS family, whereas the  $\beta$  subunit contains a series of ankyrin repeats. The crystal structure of a ternary complex containing a GABP $\alpha/\beta$  ETS domain–ankyrin repeat heterodimer bound to DNA was determined at 2.15 angstrom resolution. The structure shows how an ETS domain protein can recruit a partner protein using both the ETS domain and a carboxyl-terminal extension and provides a view of an extensive protein-protein interface formed by a set of ankyrin repeats. The structure also reveals how the GABP $\alpha$  ETS domain binds to its core GGA DNA-recognition motif.

Gene expression in eukaryotes is frequently mediated by multiprotein complexes that bind DNA in a sequence-specific manner. This type of transcriptional regulation, termed combinatorial control, is a hallmark of gene regulation in eukaryotic cells. The multiprotein complexes that control eukaryotic gene expression may be composed of structurally similar proteins, such as the Fos and Jun bZIP heterodimer (1) or the yeast MAT $\alpha$ 1/MAT $\alpha$ 2 homeodomain complex (2). In many other cases, genes are regulated by complexes composed of proteins from different structural families. Examples include the complex formed by the MAT $\alpha$ 2 homeodomain protein with the MCM1 MADS box protein (3), and by the herpes simplex VP16 transactivator protein with both the Oct-1 POU-domain protein and host cell factor (4). Understanding how transcriptional regu-

lators recruit their partners to form tight, highly specific complexes is central to an understanding of combinatorial control of transcription.

ETS domain proteins make up a large family of DNA-binding proteins found in organisms ranging from fruit flies to humans that play a role in a variety of developmental pathways, in oncogenesis, and in viral gene expression (5). These proteins have in common a conserved DNA-binding domain whose structure, as determined for the ETS proteins Fli-1, Ets-1, and PU.1, has an overall topology similar to that of the “winged helix-turn-helix” family of proteins (6–9). ETS domains bind DNA as monomers and recognize a consensus sequence that contains a core GGA motif. In many cases, greater DNA target specificity is achieved by the cooperative binding of ETS family members with partner proteins (5). For example, the related ETS proteins Elk-1, SAP-1, and SAP-2 interact with the serum response factor at the serum response element in the c-Fos promoter (10), and the ETS protein PU.1 interacts with Pip on several immunoglobulin light-chain enhancers (11).

GA-binding protein (GABP) is a cellular heteromeric DNA-binding protein

involved in the activation of nuclear genes encoding mitochondrial proteins (12), adenovirus early genes (13), and herpes simplex virus immediate-early genes (14). The GABP complex is composed of two subunits: an ETS family member, GABP $\alpha$ , and an ankyrin repeat-containing protein, GABP $\beta$  (13, 15). Ankyrin repeats, typically 33 amino acids in length, occur in multiple copies in a functionally diverse array of proteins that includes the yeast cell cycle control proteins cdc10/SWI6; the Notch transmembrane protein of *Drosophila melanogaster*; the erythrocyte membrane-associated protein, ankyrin; and I $\kappa$ B, an inhibitor of the transcription factor NF- $\kappa$ B (16). GABP $\beta$  contains four-and-a-half ankyrin repeats at its NH $_2$ -terminus that mediate heterodimerization with GABP $\alpha$  (17). Formation of the GABP $\alpha/\beta$  heterodimer requires both the GABP $\alpha$  ETS domain and 31 amino acids immediately COOH-terminal to the ETS domain (17). The GABP $\alpha/\beta$  heterodimer binds to DNA sequences containing a core GGA motif with greater affinity than the GABP $\alpha$  subunit alone (17, 18). Two GABP $\alpha/\beta$  heterodimers associate via the COOH-terminal residues of GABP $\beta$ , resulting in a heterotetramer that binds to DNA sequences containing two tandem repeats of the GGA motif (19).

To investigate how the structurally dissimilar GABP  $\alpha$  and  $\beta$  subunits form a tight heterodimer with enhanced DNA-binding affinity, we determined the crystal structure of the GABP $\alpha/\beta$  ETS domain–ankyrin repeat heterodimer bound to DNA. Recombinant fragments of mouse GABP $\alpha$  and GABP $\beta$  were expressed in *Escherichia coli*, purified as a heterodimer, and crystallized bound to a 21-base pair (bp) DNA fragment (20). The structure was solved to 2.15 Å by a combination of multiple isomorphous replacement (MIR) and multiwavelength anomalous dispersion (MAD) methods (Table 1). The model of the GABP $\alpha/\beta$ -DNA ternary complex presented here contains residues 320 to 429 of GABP $\alpha$ , residues 5 to 157 of GABP $\beta$ , and all 21 bp of the DNA.

An overview of the complex (Fig. 1)

A. H. Batchelor, D. E. Piper, C. Wolberger, Department of Biophysics and Biophysical Chemistry and the Howard Hughes Medical Institute, Johns Hopkins University School of Medicine, Baltimore, MD 21205, USA.

F. Charles de la Brousse, Tularik, Two Corporate Drive, South San Francisco, CA 94080, USA.

S. L. McKnight, Department of Biochemistry, University of Texas Southwestern Medical School, Dallas, TX 75235, USA.

\*To whom correspondence should be addressed. E-mail: cynthia@groucho.med.jhmi.edu

shows GABP $\alpha$  interacting with both the 21-bp DNA fragment and GABP $\beta$ . The DNA is B form with a slight curve in the region of contact with GABP $\alpha$ . Although GABP $\beta$  lies close to the DNA, there are no direct GABP $\beta$ -DNA interactions. The GABP $\alpha$  ETS domain contains four antiparallel  $\beta$  sheets that pack against three  $\alpha$  helices and is essentially identical in topology to the nuclear magnetic resonance (NMR) structures of Fli-1 (6) and Ets-1 (8, 9) and the crystal structure of

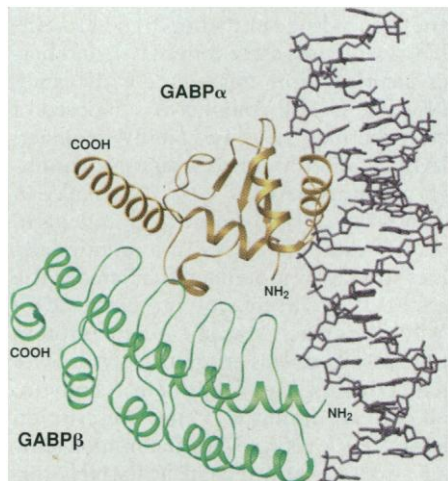


**Fig. 1.** The structure of the GABP $\alpha/\beta$ -DNA ternary complex. Ribbon diagrams of GABP $\alpha$  (gold) and GABP $\beta$  (green) are shown together with a stick model of the DNA (gray). This figure as well as Figs. 3B, 4, and 5 were prepared with SETOR (33).

PU.1 (7). The additional 31 COOH-terminal residues, required for interaction with GABP $\beta$ , form a short  $\alpha$  helix (helix 4) connected by a turn to a second  $\alpha$  helix (helix 5) that extends away from the GABP $\alpha$ -DNA interface (Figs. 1 and 2).

The GABP $\beta$  NH $_2$ -terminal domain consists of four-and-a-half ankyrin repeats arranged in tandem. The overall structure of the ankyrin repeats is very similar to that reported for 53BP2 and p19<sup>Ink4d</sup> (21, 22). Each ankyrin repeat consists of a pair of  $\alpha$  helices that form an antiparallel coiled-coil, followed by an extended loop that lies perpendicular to the helices and contains a type I  $\beta$  turn at its tip. Adjacent loops are held together by a series of side-chain and main-chain hydrogen bonds (21). Coiled-coils from neighboring repeats associate via hydrophobic interactions to form a four-helix bundle. The helix adjacent to the loop presents mostly short residues to the helix bundle, whereas the residues from the helix on the face opposite to the loop are longer (not shown). This asymmetry gives rise to a distinct curvature in the packing arrangement of adjacent ankyrin-repeat helices. As a result, the tips of the loops form a concave surface that curves around one side of GABP $\alpha$  (Fig. 3A).

The ankyrin repeats in GABP $\beta$  contact GABP $\alpha$  by inserting the tip of each loop into a depression on the side of GABP $\alpha$  that lies between the first helix of the ETS domain and the two COOH-terminal helices (Fig. 3A). Residues in the NH $_2$ - and COOH-

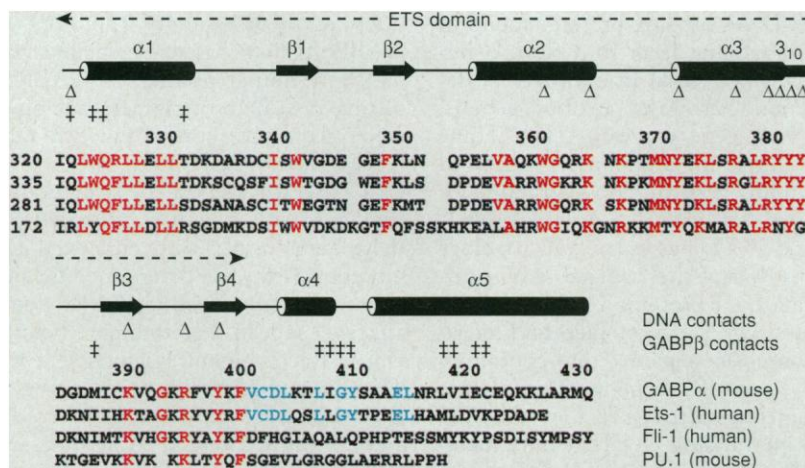


**Fig. 2.** Sequence of the GABP $\alpha$  ETS domain and COOH-terminal helices. The sequence of GABP $\alpha$  is shown together with the sequences of ETS proteins Ets-1, Fli-1, and PU.1. The numbers across the top refer to the GABP $\alpha$  sequence, with the numbers of the initial residue given for other sequences. Highly conserved residues in all ETS domains are colored red. Residues that are identical COOH-terminal to the ETS domain in GABP $\alpha$  and Ets-1 are colored blue. Secondary-structure elements are indicated by cylinders ( $\alpha$  helices) and arrows ( $\beta$  sheets). The third helix terminates with a short region of 3 $_10$  helix. Amino acid side chains that hydrogen bond to the DNA ( $\Delta$ ) as well as residues at the GABP $\beta$  interface ( $\ddagger$ ) are indicated. Abbreviations for the amino acid residues are as follows: A, Ala; C, Cys; D, Asp; E, Glu; F, Phe; G, Gly; H, His; I, Ile; K, Lys; L, Leu; M, Met; N, Asn; P, Pro; Q, Gln; R, Arg; S, Ser; T, Thr; V, Val; W, Trp; and Y, Tyr.

terminal helices of GABP $\alpha$ , as well as in the loop joining ETS domain helix 3 to  $\beta$  strand 3, form direct contacts with the  $\beta$  subunit (Figs. 2 and 3B). The interface between GABP $\alpha$  and  $\beta$  has a total buried surface area of 1600  $\text{\AA}^2$  (23) and consists primarily of complementary hydrophobic surfaces with several direct and water-mediated hydrogen bonds that presumably add specificity to the interaction. It is principally the two residues at the tip of each ankyrin repeat loop that interact with GABP $\alpha$  (Fig. 3B). Additional contacts with GABP $\alpha$  are mediated by GABP $\beta$  residues adjacent to the tips of the loops and in the ankyrin-repeat helices (Fig. 3B). A comparison with the 53BP2-p53 complex structure shows that, whereas the interaction between 53BP2 and p53 is mediated largely by the Src homology 3 (SH3) domain of 53BP2, the one region of contact with the ankyrin repeats is with the tip of the COOH-terminal ankyrin repeat loop (21). The mediation of protein-protein interactions by the tips of the loops in both the GABP $\beta$  and 53BP2 structures suggests that the tips of ankyrin-repeat loops

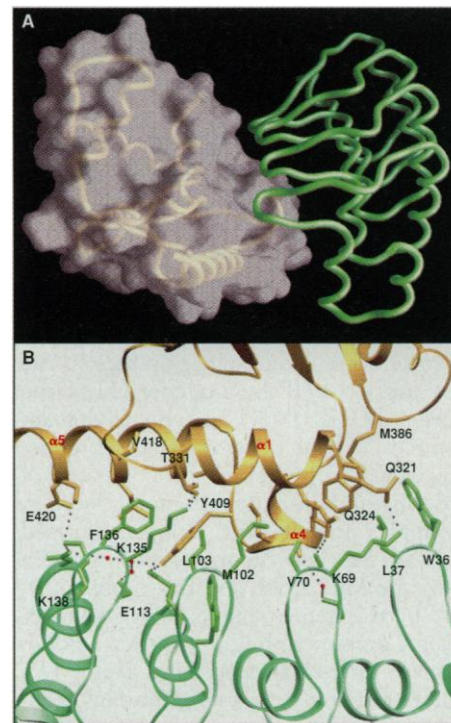


**Fig. 3.** The interaction interface between GABP $\alpha$  and GABP $\beta$ . (A) The ankyrin-repeat loops of GABP $\beta$  insert into a depression on the side of GABP $\alpha$ . The molecular surface of GABP $\alpha$  is shown together with backbone traces of GABP $\alpha$  (gold) or GABP $\beta$  (green). This figure was prepared with GRASP (34). (B) Residues at the GABP  $\alpha/\beta$  interface. Buried water molecules are shown as red spheres.  $\alpha$ 1,  $\alpha$ 4, and  $\alpha$ 5 indicate the numbering of the helices in GABP $\alpha$  (Fig. 2).

may form the principal protein-protein interaction surface of other ankyrin-repeat proteins.

The extensive involvement of the COOH-terminal extension of GABP $\alpha$  in the interaction interface with GABP $\beta$  explains why this portion of GABP $\alpha$  is required along with the ETS domain to obtain heterodimerization (17). The GABP $\beta$  interface is highly specific for GABP $\alpha$  because even Ets-1, which has a similar COOH-terminal extension (Fig. 2), fails to form a complex with GABP $\beta$  (24, 25). Although nearly all residues at the GABP $\alpha$  interface are conserved in Ets-1, the few differences would give rise to less-than-optimal contacts between Ets-1 and GABP $\beta$  (26). However, the conservation of most of the GABP $\beta$ -interacting residues in Ets-1 raises the possibility that Ets-1 may bind to an as yet unidentified GABP $\beta$ -like protein.

GABP $\alpha$  contacts DNA bases with amino acid side chains in helix 3, which lies in the major groove of the DNA and forms both direct and water-mediated hydrogen bonds with the sequence GGAA at the center of the GABP $\alpha$  recognition motif (Fig. 4A). The DNA bends toward the recognition helix with an overall curvature of 18° (27), thereby maximizing the region of contact with GABP $\alpha$ . The arginine residues that are conserved among

ETS family members, Arg<sup>379</sup> and Arg<sup>376</sup> (Fig. 2), participate in bidentate hydrogen bonding with the guanines in the core GGA motif (G8 and G9, respectively) (Fig. 4A). These contacts readily explain why the two guanine residues are essential for most ETS proteins to bind to DNA (5). The preference for an adenine residue in the core GGA motif may arise from favorable interactions mediated by the methyl group of the thymine base on the

opposing strand. The methyl group of thymine 34 fills a pocket at the surface of GABP $\alpha$  that results in a series of favorable van der Waals contacts with side-chain and main-chain atoms in Lys<sup>373</sup> and Arg<sup>376</sup> (not shown). GABP $\alpha$  makes DNA backbone contacts 3' of the GGA recognition motif with helices 1 and 2 and contacts phosphates 5' of the GGA motif with  $\beta$  strands 3 and 4 (Fig. 2, not shown). The observed phosphate contacts are con-

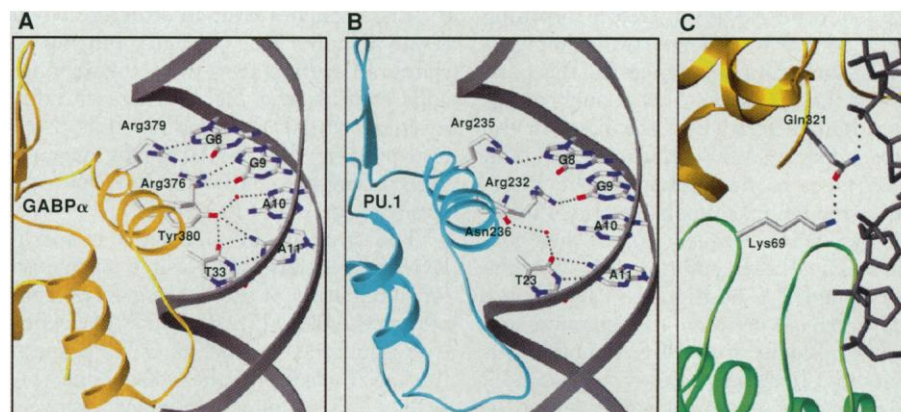


**Fig. 4.** GABP $\alpha$ -DNA interactions. **(A)** GABP $\alpha$ -DNA interactions in the major groove. Only bases making hydrogen bond contacts with GABP $\alpha$  are shown. **(B)** Interactions between the recognition helix of PU.1 and the major groove (7). **(C)** Indirect GABP $\beta$ -DNA interaction mediated by Lys<sup>69</sup> of GABP $\beta$  and Gln<sup>321</sup> of GABP $\alpha$ .

**Table 1.** Crystals of the GABP $\alpha$ / $\beta$ -DNA complex formed in space group C2 with unit cell dimensions  $a = 201 \text{ \AA}$ ,  $b = 34.6 \text{ \AA}$ ,  $c = 59.5 \text{ \AA}$ ,  $\beta = 99.9^\circ$ , with a single ternary complex in the crystallographic asymmetric unit and a solvent content of 50%. DNA derivatives were synthesized containing five bromine atoms (5Br) and one (1I) or two (2I.1, 2I.2) iodine atoms. The mercury derivative (2Hg) was prepared by soaking crystals in EMTS (20). Diffraction data sets were collected with an  $R$ -axis Ilc detector and Cu K $\alpha$ . A MAD data set was collected at beamline X-4A of the National Synchrotron Light Source at Brookhaven National Laboratory. Diffraction images were processed with DENZO and SCALEPACK (35). Data sets were scaled with SCALEIT, phases calculated with MLPHARE, and solvent-flattening carried out with DM (36).

For the MAD data sets, phases were determined independently and combined with MIR phases with SIGMAA (36). Inclusion of MAD phases resulted in a slight improvement in the 2.8  $\text{\AA}$  experimental map. An initial model was built with O (37). The model was refined with X-PLOR (23) to 2.15  $\text{\AA}$  against the 5Br ( $\lambda$ 1) data set, incorporating constrained individual  $B$  factor and anisotropic overall  $B$  factor refinements. Ten percent of the data were excluded from refinement calculations for  $R_{\text{free}}$  determination. Refined  $B$  factors for the DNA were relatively high in regions not contacting GABP $\alpha$ . It was therefore necessary to constrain DNA backbone torsion angles at certain residues at nonprotein contacted positions. The model was confirmed with simulated-annealing omit maps. rms, root mean square.

	Native	5Br	1I	2I.1	2I.2	2Hg	5Br ( $\lambda$ 1)	5Br ( $\lambda$ 2)	5Br ( $\lambda$ 3)	5Br ( $\lambda$ 4)	
Wavelength ( $\text{\AA}$ )	1.54	1.54	1.54	1.54	1.54	1.54	0.9270	0.9203	0.9196	0.9102	
Resolution ( $\text{\AA}$ )	30–2.8	30–2.8	30–2.8	30–2.8	30–2.4	30–2.4	30–2.15	30–2.15	30–2.15	30–2.15	
Redundancy (mates separated)	5.3	6.4	7.6	7.1	8.0	6.5	8.7	(4.4)	(4.4)	(4.4)	
Completeness (%) (outer shell)	100 (100)	100 (99)	100 (100)	100 (99)	100 (100)	100 (100)	88 (88)	88 (90)	88 (90)	88 (91)	
Overall $I/\sigma(I)$ (outer shell)	17 (6.9)	9.8 (8.6)	18 (6.0)	18 (5.5)	19 (5.1)	12 (5.2)	21 (5.3)	21 (5.1)	21 (5.2)	21 (5.0)	
$R_{\text{sym}}$ (%) (outer shell)	7.3 (20)	5.8 (14)	5.8 (14)	5.8 (14)	7.4 (30)	9.3 (26)	7.2 (22)	7.5 (22)	7.5 (23)	7.4 (23)	
		<i>MIR phasing (15–2.8 <math>\text{\AA}</math>)</i>						<i>MAD phasing (15–2.8 <math>\text{\AA}</math>)</i>			
$R_{\text{iso}}$ (%)	-	11.1	13.6	10.8	12.5	16.4	1.9	-	1.4	2.1	
$R_{\text{cullis}}$ (acentric)	-	0.82	0.87	0.82	0.85	0.77	0.92	-	0.96	0.91	
$R_{\text{cullis}}$ , anomalous	-	-	0.98	0.96	0.94	0.97	-	0.93	0.90	0.91	
Phasing power (acentric)	-	1.21	0.91	1.17	1.06	1.33	0.74	-	0.50	0.77	
Mean figure of merit	0.65							0.35			
Mean figure of merit (MIR and MAD combined)		0.68									
		<i>Refinement [with 5Br (<math>\lambda</math>1) data set]</i>									
Resolution range	6–2.15 $\text{\AA}$										
$R_{\text{factor}}$ (%)	21.1 ( $F > 2\sigma$ )		22.2 (all $F$ )								
$R_{\text{free}}$ (%)	28.2 ( $F > 2\sigma$ )		29.2 (all $F$ )								
rms deviations	Bonds 0.007 $\text{\AA}$		Angles 1.17°								
Average $B$ ( $\text{\AA}^2$ )	25.7 GABP $\alpha$		30.5 GABP $\beta$			51.2 DNA			27.6 solvent atoms		
18368 reflections ( $17217 > 2\sigma$ )	2966 atoms		46 solvent atoms								

sistent with ethylation interference footprinting of GABP $\alpha/\beta$  on DNA (28).

The contacts formed by GABP $\alpha$  with DNA differ in some notable respects from those observed in the x-ray crystal structure of the minimal ETS domain of PU.1 bound to DNA (7). PU.1 is one of the most evolutionarily divergent members the ETS family (Fig. 2), and some of the PU.1-DNA-contacting residues are not conserved in GABP $\alpha$ . Nevertheless, most DNA backbone contacts observed for GABP $\alpha$  are identical in the PU.1 structure (Fig. 2, not shown). It is therefore surprising that a comparison of the two complexes reveals significant differences in the positions of the respective ETS domain recognition helices relative to the bases in the major groove. A 1.5 Å shift in the relation of the bases to the protein in the PU.1-DNA structure makes possible only a single hydrogen bond between Arg<sup>235</sup> and guanine 8 (Fig. 4B). In addition, Arg<sup>232</sup> in the PU.1 complex is positioned such that the NH1 atom is between the guanine and adenine residues of the GGA motif. This results in a hydrogen bond with guanine 9 (O6) and a close contact with adenine 10 (N6). Although these differences are surprising, they are partly consistent with the observation that PU.1 is unusual amongst ETS proteins in that it is able to recognize an AGA motif in addition to the GGA core motif (29).

The structures that have been reported for PU.1 (7) and Ets-1 (8) complexed with DNA contain only the minimal ETS domain. However, the structure of uncomplexed Ets-1 containing the COOH-terminal extension that is conserved in both GABP $\alpha$  and Ets-1 has been determined by solution NMR (9). Comparison of the backbone topology of GABP $\alpha$  with Ets-1 reveals a marked difference between the two proteins in the positioning of the COOH-terminal helix relative to the ETS domain (Fig. 5). In the GABP $\alpha/\beta$  complex, helix 5 of GABP $\alpha$  forms only a few contacts with the ETS domain and extends away from the protein-DNA interface (Fig. 1). In contrast, the structure of uncomplexed Ets-1 shows that the corresponding COOH-terminal extension

points in the opposite direction, allowing the COOH-terminal helix to pack against helix 1 of the ETS domain. This packing buries hydrophobic residues in both the COOH-terminal tail and the ETS domain of Ets-1. These residues correspond to hydrophobic residues in GABP $\alpha$  that are contacted by GABP $\beta$ . The fact that these residues are conserved in both Ets-1 and GABP $\alpha$  (Fig. 2) suggests that, in the absence of GABP $\beta$ , the COOH-terminal extension of GABP $\alpha$  may also pack against the ETS domain in the manner observed for Ets-1. Such a shift in structure would result in helix 5 of GABP $\alpha$  pointing toward, rather than away from, the region of contact with the DNA where it could interfere with DNA binding. It is therefore possible that GABP $\beta$  may augment the binding of GABP $\alpha$  to DNA by reorientating helix 5 of GABP $\alpha$ .

The structure of GABP $\alpha/\beta$  bound to DNA suggests another possible mechanism for stabilization of the GABP $\alpha$ -DNA complex by GABP $\beta$  (17, 18). Gln<sup>321</sup> of GABP $\alpha$  hydrogen bonds to Lys<sup>69</sup> of GABP $\beta$  and to the DNA sugar-phosphate backbone (Fig. 4C). This indirect contact between GABP $\beta$  and the DNA, in addition to the reorientation of the COOH-terminal helix of GABP $\alpha$ , may explain the slower rate of dissociation from DNA observed for GABP $\alpha/\beta$  as compared to GABP $\alpha$  alone (17, 18).

Full-length Ets-1 binds to DNA less efficiently than truncated Ets-1 variants lacking residues on either side of the ETS domain. This inhibition of DNA binding is a consequence of the association of the COOH-terminal residues with a helix-containing domain that lies NH<sub>2</sub>-terminal to the ETS domain (30, 31). Whereas the COOH-terminal extension is conserved in both Ets-1 and GABP $\alpha$ , the NH<sub>2</sub>-terminal helix domain is not. However, comparison of the GABP $\alpha/\beta$  and Ets-1 structures is highly suggestive of a mechanism by which an auxiliary factor could relieve the inhibition of DNA binding observed for Ets-1. Binding of an auxiliary factor in a manner analogous to GABP $\beta$  would result in a shift in the COOH-terminal helix of Ets-1, thereby disrupting the interaction

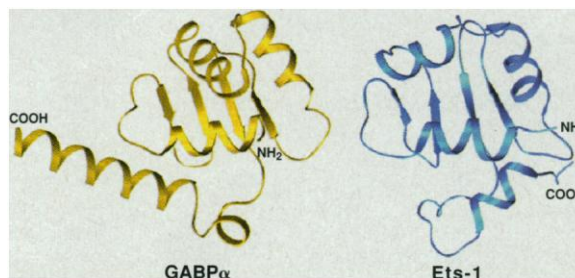
with the NH<sub>2</sub>-terminal domain and relieving inhibition of DNA binding.

Complex formation between the GABP $\alpha$  ETS domain protein and the GABP $\beta$  ankyrin-repeat protein is just one of a number of known examples of ternary complexes involving ETS domain proteins and structurally different partners. Biochemical evidence would suggest that other ETS proteins have evolved different mechanisms by which they recruit other proteins (10, 32), which may be a consequence of the structural diversity of their protein partners. The GABP $\alpha/\beta$  complex also reveals a mechanism by which a series of ankyrin repeats can interact with their partner protein. The modular manner by which successive loops interact with GABP $\alpha$  is highly suggestive of an evolutionary process in which the duplication of a repeat followed by mutation of the residues at the tips of the loops would allow for the progressive alteration of the specificity or affinity of an interaction. The facility by which an ankyrin repeat domain could evolve new protein target specificities may explain why ankyrin repeats are frequently involved in protein-protein interactions.

## REFERENCES AND NOTES

1. J. N. M. Glover and S. C. Harrison, *Nature* **373**, 257 (1995).
2. T. Li, M. R. Stark, A. D. Johnson, C. Wolberger, *Science* **270**, 262 (1995).
3. C. A. Keleher, C. Goutte, A. D. Johnson, *Cell* **53**, 927 (1988).
4. C. C. Thompson and S. L. McKnight, *Trends Genet.* **8**, 232 (1992).
5. B. J. Graves and J. M. Petersen, in *Advances in Cancer Research*, G. van de Woude and G. Klein, Eds. (Academic Press, San Diego, CA, in press).
6. H. Liang et al., *Nature Struct. Biol.* **1**, 871 (1994).
7. R. Kodandapani et al., *Nature* **380**, 456 (1995).
8. M. H. Werner et al., *Cell* **83**, 761 (1995) [published erratum *Cell* **87**, following 355 (1996)].
9. L. W. Donaldson, J. M. Petersen, B. J. Graves, L. P. McIntosh, *EMBO J.* **15**, 125 (1996).
10. M. A. Price, A. E. Rogers, R. Treisman, *ibid.* **14**, 2589 (1995).
11. C. F. Eisenbeis, H. Singh, U. Storb, *Genes Dev.* **9**, 1377 (1995).
12. J. V. Virbasius, C. A. Virbasius, R. C. Scarpulla, *ibid.* **7**, 380 (1993).
13. H. Watanabe et al., *Mol. Cell. Biol.* **13**, 1385 (1993).
14. S. J. Triezenberg, K. L. LaMarco, S. L. McKnight, *Genes Dev.* **2**, 730 (1988).
15. K. LaMarco, C. C. Thompson, B. P. Byers, E. M. Walton, S. L. McKnight, *Science* **253**, 789 (1991).
16. V. Bennett, *J. Biol. Chem.* **267**, 8703 (1992).
17. C. C. Thompson, T. A. Brown, S. L. McKnight, *Science* **253**, 762 (1991).
18. In DNA dissociation experiments with the minimal fragments used in this study, GABP $\alpha$  dissociated with a half-life of less than 4 s, whereas the half-life of GABP $\alpha/\beta$  was ~400 s.
19. F. Charles de la Brousse, E. H. Birkenmeier, D. S. King, L. B. Rowe, S. L. McKnight, *Genes Dev.* **8**, 1853 (1994).
20. Two GABP $\beta$  genes have been identified, GABP $\beta$ 1 and GABP $\beta$ 2 (19). In this study we used GABP $\beta$ 1. Residues 311 to 430 of GABP $\alpha$  and 1 to 157 of GABP $\beta$  expressed as precipitates in *E. coli*. The proteins were codialyzed from 8 M urea, purified as

**Fig. 5.** Comparison of the GABP $\alpha$  crystal structure and Ets-1 NMR structure (9). Each structure is positioned with its ETS domain in the same orientation.



- a complex by anion- and cation-exchange chromatography, and concentrated to 8 mg/ml. Purified AATGACCGGAAGTACACCGGA and TTCCGGTGTACTCCGGTCAT 21-base oligonucleotides were added to protein in slight molar excess and dialyzed into 20 mM tris (pH 8), 1 mM EDTA, 1 mM dithiothreitol, and 0.001% sodium azide. Equal volumes of protein-DNA solution and well solution [100 mM bis-tris propane (pH 9), 5 mM cobaltic hexamine chloride, 9% polyethylene glycol (PEG) 1000] were mixed, and hanging drops were allowed to equilibrate by vapor diffusion at 20°C. Crystals were transferred into cryosolutions containing well solution with 12% PEG 1000 and 24% glycerol. Optimal diffraction was obtained if crystals were cross-linked by exposure to glutaraldehyde vapor for 10 min. For the 2Hg derivative, a cross-linked crystal was soaked in 1 mM EMTS (ethylmercurithiosalicylate) for 24 hours.
21. S. Gorina and N. P. Pavletich, *Science* **274**, 1001 (1996).
  22. F. Y. Luh *et al.*, *Nature* **389**, 999 (1997).
  23. A. T. Brünger, *X-PLOR, version 3.1, A System for X-Ray Crystallography and NMR* (Yale Univ. Press, New Haven, CT, 1992).
  24. T. A. Brown and S. L. McKnight, *Genes Dev.* **6**, 2502 (1992).
  25. Ets-1 fragments  $\Delta$ N331 or  $\Delta$ N280 (31) did not interact with GABPB 1 or 2 in electrophoretic mobility-shift assays when mixed or codialyzed from 8 M urea.
  26. In a model of Ets-1 bound to GABP $\alpha$ , the substitution of valine for Glu<sup>420</sup> disrupts a hydrogen bond and the substitution leucine for Val<sup>418</sup> results in a steric clash with neighboring hydrophobic residues.
  27. Curvature of the DNA was calculated for the 9 bp contacting GABP $\alpha$  with the program CURVES; R. Lavery and H. Sklenar, *J. Biomol. Struct. Dyn.* **6**, 63 (1988).
  28. C. V. Gunther and B. J. Graves, *Mol. Cell. Biol.* **14**, 7569 (1994).
  29. M. K. Shin and M. E. Koshland, *Genes Dev.* **7**, 2006 (1993).
  30. J. J. Skaliky, L. W. Donaldson, J. M. Petersen, B. J. Graves, L. P. McIntosh, *Protein Sci.* **5**, 296 (1996).
  31. J. M. Petersen *et al.*, *Science* **269**, 1866 (1995).
  32. D. Fitzsimmons *et al.*, *Genes Dev.* **10**, 2198 (1996).
  33. S. V. Evans, *J. Mol. Graph.* **11**, 134 (1993).
  34. A. Nicholls, K. Sharp, B. Honnig, *Proteins* **11**, 281 (1991).

35. Z. Otwinowski, in *Proceedings of the CCP4 Study Weekend: Data Collection and Processing*, L. Sawyer, N. Isaacs, S. Bailey, Eds. (Science and Engineering Research Council Daresbury Laboratory, Warrington, UK, 1993), pp. 56–62.
36. Collaborative Computational Project Number 4, *Acta Crystallogr.* **D50**, 760 (1994).
37. T. A. Jones, J. Y. Zou, S. W. Cowan, M. Kjeldgaard, *ibid.* **A47**, 110 (1991).
38. We thank S. Soisson and E. Reisinger for continuous assistance; S. Prigge, D. Hammontree, and D. Leahy for programs; M. Bianchet and M. Amzel for x-ray room assistance; C. Ogata for beamline assistance; N. Pavletich for 53BP2 coordinates; and B. Graves for Ets-1 samples. This work was initiated during a sabbatical visit by S.L.M. in the laboratory of C.W. At that time S.L.M. was supported by the Carnegie Institute of Washington and the Howard Hughes Medical Institute. A.H.B., D.E.P., and C.W. were supported by the Howard Hughes Medical Institute. C.W. also received support from the David and Lucile Packard Foundation. Coordinates have been deposited at the Brookhaven Protein Data Bank (accession code 1awc).

18 August 1997; accepted 18 December 1997

## Budding Yeast Cdc20: A Target of the Spindle Checkpoint

Lena H. Hwang, Lucius F. Lau, Dana L. Smith, Cathy A. Mistrot, Kevin G. Hardwick,\* Ellen S. Hwang, Angelika Amon, Andrew W. Murray†

The spindle checkpoint regulates the cell division cycle by keeping cells with defective spindles from leaving mitosis. In the two-hybrid system, three proteins that are components of the checkpoint, Mad1, Mad2, and Mad3, were shown to interact with Cdc20, a protein required for exit from mitosis. Mad2 and Mad3 coprecipitated with Cdc20 at all stages of the cell cycle. The binding of Mad2 depended on Mad1 and that of Mad3 on Mad1 and Mad2. Overexpression of Cdc20 allowed cells with a depolymerized spindle or damaged DNA to leave mitosis but did not overcome the arrest caused by unrepllicated DNA. Mutants in Cdc20 that were resistant to the spindle checkpoint no longer bound Mad proteins, suggesting that Cdc20 is the target of the spindle checkpoint.

The spindle checkpoint improves the fidelity of chromosome segregation by delaying anaphase until all chromosomes are correctly aligned on the mitotic spindle (1, 2). Mutants in the MAD (mitosis arrest deficient) and BUB (budding uninhibited by benzimidazole) genes inactivate the checkpoint (3, 4), and overexpressing components of the checkpoint can arrest cells with normal spindles in mitosis (5–7). The checkpoint prevents ubiquitination and destruction of at least two types

of protein: the B-type cyclins, which activate the protein kinase activity of cyclin-dependent kinase (Cdk1, known as Cdc28 in budding yeast and Cdc2 in fission yeast), and a protein required to maintain the linkage of sister chromatids (Pds1 in budding yeast and Cut2 in fission yeast) (8–11). Ubiquitination is catalyzed by a multiprotein complex called the cyclosome or anaphase promoting complex (APC) (12–14). The reactions that activate the APC are not understood, but cyclin B and Pds1/Cut2 destruction depends on Cdc20 and Hct1/Cdh1, two evolutionarily conserved members of the WD (Trp-Asp) repeat family of proteins. Cdc20 preferentially promotes the destruction of Pds1/Cut2, and Hct1 promotes the destruction of B-type cyclins (15, 16). Unlike HCT1, CDC20 is an essential gene, and temperature-sensitive *cdc20* mutants arrest in metaphase.

The interaction between Slp1 (the homolog of Cdc20) and Mad2 in fission yeast (7) prompted us to investigate the interaction between Cdc20 and components of the spindle assembly checkpoint in budding yeast. In the two-hybrid system, Mad1, Mad2, and Mad3 all showed interactions with Cdc20 (Fig. 1A), suggesting that checkpoint proteins bind to Cdc20. We confirmed this suggestion by immunoprecipitating an epitope-tagged version of Cdc20 and probing the immunoprecipitates with antibodies to Mad2 and Mad3 (17). We examined four conditions: cells growing asynchronously, cells arrested in G<sub>1</sub>, cells arrested in mitosis by depolymerization of the spindle with nocodazole, and cells arrested in mitosis by *cdc26* $\Delta$ , a mutant that inactivates the APC (18, 19). Both Mad2 and Mad3 were present in immunoprecipitates from strains carrying epitope-tagged Cdc20 (Fig. 1B). We were unable to monitor the physical interaction between Mad1 and Cdc20 because free Mad1 binds to antibody-coated beads in some control experiments. The amount of Mad2 and Mad3 precipitated with Cdc20 was highest in cells arrested in mitosis, lower in asynchronous cells, and still lower in cells arrested in G<sub>1</sub>. The increased association in mitotic cells does not depend on checkpoint activation, because cells arrested by inactivation of the APC showed the same interaction between Cdc20 and Mad proteins as cells arrested in mitosis by spindle depolymerization. We suspect that the different levels of Mad-Cdc20 association between mitotic and G<sub>1</sub> cells reflect the level of Cdc20, which is high in mitosis and low in G<sub>1</sub> (20).

Because two Mad proteins associate with Cdc20, we asked whether they asso-

L. H. Hwang, D. L. Smith, C. A. Mistrot, K. G. Hardwick, A. W. Murray, Departments of Physiology and Biochemistry, University of California at San Francisco, San Francisco, CA 94143–0444, USA.

L. F. Lau, E. S. Hwang, A. Amon, Whitehead Institute for Biomedical Research, 9 Cambridge Center, Cambridge, MA 02142, USA.

\*Present address: Institute of Cell and Molecular Biology, University of Edinburgh, Edinburgh, EH9 3JR, UK.

†To whom correspondence should be addressed. E-mail: amurray@socrates.ucsf.edu